Journal of Hazardous Materials Letters 2 (2021) 100007

Contents lists available at ScienceDirect

Journal of Hazardous Materials Letters

journal homepage: www.elsevier.com/locate/hazl

Redox-active rGO-nZVI nanohybrid-catalyzed chain shortening of perfluorooctanoic acid (PFOA) and perfluorooctane sulfonic acid (PFOS)

Arvid Masud [a,1], Mary Grace E. Guardian [b,1], Steven C. Travis [b], Nita G. Chavez Soria [b], Mourin Jarin [c], Diana S. Aga [b,*], Nirupam Aich [a,*]

[a] Department of Civil, Structural and Environmental Engineering, University at Buffalo, The State University of New York, Buffalo, NY 14260, United States
[b] Department of Chemistry, University at Buffalo, The State University of New York, Buffalo, NY 14260, United States
[c] Department of Chemical and Biological Engineering, University at Buffalo, The State University of New York, Buffalo, NY 14260, United States

ARTICLE INFO

Keywords:
Per- and polyfluoroalkyl substances (PFASs)
Advanced oxidation process
Heterogeneous fenton reactions
Graphene
Nanomaterial-enabled treatment

ABSTRACT

Per- and polyfluoroalkyl substances (PFASs) are exceptionally stable chemicals due to their strong C—F bonds. Nanoscale zero-valent iron (nZVI) particles have the potential to remove and degrade PFASs through redox activity. In this study, we deposited nZVI onto two-dimensional reduced graphene oxide (rGO) nanosheets and tested these synthesized rGO-nZVI nanohybrid (NH) for the treatment of a mixture of short- and long-chain PFASs in water with and without H_2O_2. All PFASs were removed at a higher efficiency by the rGO-nZVI NH than by the parent materials rGO and nZVI. Notably, the long-chain PFASs were removed at a faster rate than the short-chain PFASs. After a 10 min exposure to the rGO-nZVI NH without H_2O_2, the long-chain PFASs (perfluorooctane sulfonic acid (PFOS) and perfluorooctanoic acid (PFOA)) were removed by 85 % and 39 %, respectively, while short-chain PFASs (perfluoropentane sulfonic acid and perfluoropentanoic acid) were removed by 19 % and 18 %, respectively. The addition of H_2O_2 enhanced the PFAS treatment performance by 10–18 %, which can be attributed to the generation of reactive oxygen species by the rGO-nZVI NH. Liquid chromatography high-resolution mass spectrometry analysis confirmed the formation of unique shorter chain and partially defluorinated PFAS-Fe complexes from both PFOS and PFOA.

1. Introduction

Per- and polyfluoroalkyl substances (PFASs) are synthetic chemicals characterized by strong C—F bonds, and the presence of a hydrophobic carbon chain and a hydrophilic head group. PFASs possess exceptional properties suitable for a wide range of uses in commercial products and various industrial applications (e.g., non-stick coating, fire-fighting foams, food packaging) (Kucharzyk et al., 2017,Kim et al., 2015, Gallen et al., 2018). These unique physicochemical properties also cause PFASs to be persistent and bio-accumulative in the environment, leading to their frequent detection in drinking water sources worldwide (Gui et al., 2019, Post et al., 2013, Kaboré et al., 2018, Guardian et al., 2020) The toxicological effects of PFAS are wide ranging, and include endocrine disruption, cancer, immunotoxicity, and developmental delay to name a few (Hekster et al., 2003, DeWitt, 2015, Lau et al., 2006). Therefore, the development of effective treatment technologies for the removal of PFASs from the environment is warranted.

Recently, different nanomaterial-enabled treatment techniques have been studied for removing PFASs from water (Saleh et al., 2019; Zhang et al., 2019a). Many of these approaches involve non-destructive phase transfer (e.g., adsorption, filtration) of PFASs from water resulting from the high surface area of nanomaterials (Deng et al., 2012, Meng et al., 2014, Gao and Chorover, 2012a). However, the ultimate outcome desired from utilizing nanomaterials is to transform or degrade PFASs into non-toxic by-products. Studies that attempted to transform or degrade PFASs using nanomaterials have used photocatalytic (Chen et al., 2011), electrochemical (Xue et al., 2015), or microwave-assisted setups (Li et al., 2017) that require high energy input.

Nanoscale zero-valent iron (nZVI; Fe°) is the most used nanomaterial for contaminated soil and water remediation in the United States Zhao et al., 2016a, and is a promising candidate for PFAS removal via both adsorption and degradation. Recently, surface-modified nZVI has been shown to perform reductive defluorination of PFASs due to its high reductive capacity (standard reduction potential, $E^{\circ} = -0.44$ V) (Adusei-Gyamfi and Acha, 2016). Furthermore, nZVI has been shown to perform oxidative degradation of a long-chain PFAS (perfluorooctanoic acid (PFOA)) in the presence of common oxidants e.g., hydrogen peroxide (H_2O_2) (Parenky et al., 2020). This is possible due to the ability of nZVI to

* Corresponding authors.
E-mail addresses: dianaaga@buffalo.edu (D.S. Aga), nirupama@buffalo.edu (N. Aich).
[1] Equally contributing first author.

http://doi.org/10.1016/j.hazl.2020.100007
Received 2 September 2020; Received in revised form 20 November 2020; Accepted 29 November 2020
Available online 3 December 2020

act as a heterogeneous Fenton catalyst and generate reactive oxygen species (ROS) by activating H_2O_2 without external energy input. However, neither of these above-mentioned studies identified the unknown byproducts of PFAS degradation.

In addition, the reactivity of nZVI in aqueous media is known to be hindered by their aggregation and surface passivation. One major approach of improving nZVI's reactivity is the usage of carbon-based materials as solid supports (Aich et al., 2018). Our recent studies demonstrated that hybridization of nZVI with two-dimensional carbonaceous nanomaterials such as graphene oxide (GO) or reduced graphene oxide (rGO) resulted in enhanced removal of pharmaceuticals, heavy metals, and dyes from water relative to using only nZVI (Masud et al., 2020a, Masud et al., 2018, Mehrabi et al., 2019). Conjugation of nZVI with rGO (or GO) resists nZVI's aggregation, improves nZVI's redox activity due to the presence of delocalized electrons on the rGO (or GO) nanosheets, and enhance the interaction of nZVI with the contaminants by adsorbing them on rGO (or GO) surface (Gu et al., 2018). Furthermore, GO and rGO have recently been reported as competent adsorbents for PFASs (Meng et al., 2014; Zhao et al., 2016b). Thus, the nanohybrid of rGO and nZVI, i.e., rGO-nZVI NH, has the potential to facilitate the removal of PFASs through increased adsorption, reduction, and/or advanced oxidation in the presence of H_2O_2.

This study aimed to evaluate the efficacy of PFAS removal in water by rGO-nZVI NH in comparison with that by the parent nanomaterials rGO and nZVI – both in the absence and presence of H_2O_2. To achieve this aim, a mixture of short- and long-chain PFASs in water were treated with either rGO-nZVI NH, rGO or nZVI. Subsequently, the decrease in concentrations of these PFASs in water at different time intervals were evaluated using liquid chromatography coupled to tandem mass-spectroscopy (LC–MS/MS). The tested PFASs include short-chain perfluoropentanoic acid (PFPeA; C_4F_9COOH) and perfluoropentane sulfonic acid (PFPeS; $C_5F_{11}SO_3H$), and long-chain perfluorooctanoic acid (PFOA; $C_7F_{15}COOH$) and perfluorooctane sulfonic acid (PFOS; $C_8F_{17}SO_3H$). This study also aimed to identify unknown PFAS degradation byproducts and elucidate degradation pathways. To achieve these aims, we used liquid chromatography with high-resolution mass spectroscopy (LC-HRMS) and ion chromatography (IC) to analyze PFAS solutions treated with the nanohybrids.

2. Materials and methods

The details regarding the synthesis and characterization of rGO-nZVI NH and parent materials, rGO and nZVI, were described in our previous studies (Masud et al., 2020a, Wang et al., 2018). Details about the PFAS removal experiments with the nanomaterials and quantification by LC–MS/MS analyses are provided in the supplementary information (SI, Section 1).

2.1. Determination of degradation byproducts

Individual PFOA and PFOS samples with initial concentrations of 400 μg/L were exposed to rGO-nZVI NH without and with H_2O_2 treatment, as described in Section 1.2 of the SI, and aliquots from these samples were collected immediately after nanomaterial addition and after 30 min. For determining PFOA and PFOS degradation byproducts, these aliquots, after centrifugation, were analyzed using a LC-HRMS Thermo Scientific Q-Exactive Focus™ with Thermo Scientific UltiMate 3000 UHPLC™, operated in negative electrospray ionization (-ESI). Chromatographic separation was performed using the column and mobile phases discussed in Section 1.3 of the SI. Detailed acquisition parameters for HRMS analysis were described elsewhere (Guardian et al., 2021). In addition, IC was also performed to detect formate and acetate formation during the removal tests (refer to Section S1.5 in SI for details). The presence of formate and acetate in the reaction mixture is indicative of carbon-chain shortening and hence, PFAS degradation (Singh et al., 2019). Treated PFAS solutions were also analyzed for the presence of F^- ions, however, the detection limit of the ion chromatography with a conductivity detector was too high to detect formation of F^- ions.

3. Results and discussion

3.1. Mixed PFAS removal by rGO-nZVI NH, rGO, and nZVI without and with H_2O_2

Fig. S1 presents the normalized concentrations (C/C_0) at different time intervals for the 4 PFASs in the mixed PFAS solution treated with the rGO-nZVI NH and the parent materials rGO and nZVI in the absence and presence of H_2O_2. In addition, the values of fraction removal i.e., 1- C/C_0 for all 4 PFASs after 10 min of treatment are presented in Fig. 1. The rGO-nZVI NH is presented as NH in all figures and tables onwards.

For all 4 PFASs, the rGO-nZVI NH showed a faster decrease in concentrations compared to rGO and nZVI separately, both without and with H_2O_2 (Fig. S1). Fig. 1 shows that treatment by rGO-nZVI NH results in a greater PFAS removal than by rGO and nZVI individually. For example, in the absence of H_2O_2, 84 % of PFOS is removed by rGO-nZVI NH while rGO and nZVI removed only 73 % and 65 % of PFOS, respectively. The higher removal efficiency provided by rGO-nZVI NH can be attributed to the resistance against nZVI aggregation, the resistance against restacking of rGO nanosheets, and the adsorption by rGO in the hybrid (Jang et al., 2013; Peik-See et al., 2014). Notably, PFAS removal efficiencies by the nanomaterials was dependent on the PFAS chain length and type of head group. Long-chain PFASs were better removed than short-chain PFASs, and PFASs with sulfonic acid groups were better removed than those with carboxylic acid groups (Fig. 1). The observed effects of PFAS structure (i.e., the effect of carbon-chain length or head groups) on their removal by these nanomaterials are consistent with those observed in other adsorbents, e.g., granular activated carbons (Zhang et al., 2019b) and carbon nanotubes (Deng et al., 2012). For example, PFAS removal after a 10-min exposure to rGO-nZVI NH in the absence of H_2O_2 was the highest for PFOS with 84 % removal followed by removal of 39 % PFOA, 19 % PFPeS, and 18 % PFPeA. This trend in structural dependence of PFAS removal was also true for rGO and nZVI.

The results presented in Fig. 1 also helped to elucidate the role of H_2O_2 in facilitating advanced oxidation (Masud et al., 2020a) and in enhancing PFAS removal by rGO-nZVI NH. Fe° reacts with H_2O_2 at the nZVI surface – via a two-electron transfer process – to produce surface bound Fe^{2+} ions. These Fe^{2+} ions further react with H_2O_2 to generate ROS which facilitate degradation of contaminants (Masud et al., 2020a; Xu and Wang, 2011). For the carbonaceous parent nanomaterial rGO, addition of H_2O_2 did not enhance the PFAS removal performance suggesting no catalytic activity of rGO. Rather, the removal decreased slightly (6 %–12 %) for all the 4 PFASs, which can be attributed to the competitive adsorption of H_2O_2 instead of PFASs (Düzenli, 2016, Amirfakhri et al., 2014, Majidi and

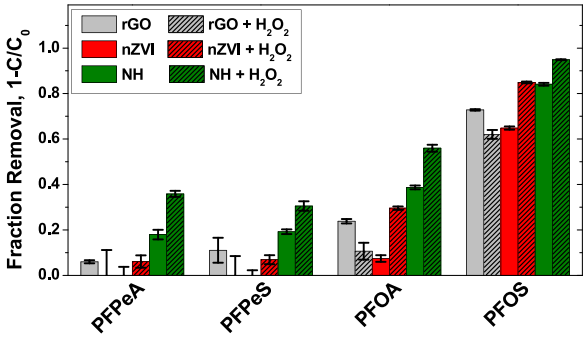

Fig. 1. Fraction removal (n = 3) of mixed PFASs i.e., PFPeA, PFPeS, PFOA, and PFOS by rGO-nZVI NH, rGO, and nZVI in the absence and presence of H_2O_2. The rGO-nZVI NH is presented as NH in the legend. [Initial concentration of individual PFASs = 200 μg/L in DI water, volume of sorbate = 10 mL, Adsorbent dose = 5 mg, pH = 3, dissolved oxygen = ~8 mg/L, ionic strength = $\sim 1 \times 10^{-7}$ M), exposure time = 10 min at room temperature].

Karami, 2014). However, the addition of H_2O_2 enhanced the performance of nZVI by 30 % and 20 % for long chain PFOA and PFOS, respectively, suggesting that nZVI acts as heterogeneous Fenton catalyst in the presence of H_2O_2. Most importantly, the rGO-nZVI NH with H_2O_2 outperformed both rGO and nZVI. In the presence of H_2O_2, rGO-nZVI NH resulted in a 95 % removal of PFOS after 10-min of treatment. In contrast, only 84 % of PFOS was removed in the absence of H_2O_2. The presence of H_2O_2 enhanced the PFAS removal efficiencies of rGO-nZVI NH after 10-min treatment by 17 % for PFOA, 12 % for PFPeS, and 18 % for PFPeA. Furthermore, the estimated pseudo first order removal rate constants (Table S2) for rGO-nZVI NH were 24–62 % higher in the presence of H_2O_2 for all 4 PFASs than that in the absence of H_2O_2.

To better understand the synergistic effects of hybridization on PFAS removal, we used the mass composition ratio of rGO and nZVI in the synthesized rGO-nZVI NH along with the individual removal efficiencies of parent rGO and nZVI to determine the expected efficiency of rGO-nZVI NH. The mass ratio of rGO and nZVI in the rGO-nZVI NH was found to be 1:3.2, as reported in our previous studies (Wang et al., 2018; Masud et al., 2020b). Fig. S2 presents the comparison of the expected efficiency (predicted additive fraction removal) and the experimental values of fraction removal by the rGO-nZVI NH, with and without H_2O_2. The experimental values were much higher than the predicted values for all four PFASs by up to 28 % and 31 % in the absence and presence of H_2O_2, respectively. This indicates that the rGO-nZVI NH produces a positive synergistic effect for enhanced PFAS removal that cannot be predicted from the additive performances of individual parent materials. Similar synergistic effect of hybridization of rGO and nZVI has been observed in our previous study with a different sorbate – a mixture of pharmaceuticals (Masud et al., 2020b).

Although different mechanisms are involved in the PFAS removal by these nanomaterials, adsorption is one of the major mechanisms responsible for the observed variability in removal efficiencies for different PFASs. Adsorption of PFASs by nanomaterials can be driven by both hydrophobic and electrostatic interactions (Li et al., 2017; Zhao et al., 2016a; Wang et al., 2018). The higher removal performance for the long chain PFASs, i.e., for PFOA and PFOS, especially by rGO-nZVI NH and rGO, relative to their short chain counterparts with same terminal functional groups (i.e., PFPeA and PFPeS, respectively) can be attributed to the hydrophobic interactions associated with the longer perfluoroalkyl chain (Li et al., 2017; Majidi and Karami, 2014). Short-chain PFPeA and PFPeS have lower octanol-water partition co-efficients, log D, (0.406 and 0.950, respectively) than long-chain PFOA and PFOS, thus are less adsorbed by the rGO-nZVI NH (Guardian et al., 2021; ChemAxon ChemAxon, 2020). The higher adsorptive removal for PFOS than for PFOA can be attributed to the higher hydrophobicity of PFOS (log D = 3.054) compared to that of PFOA (log D = 1.584) (Kelly et al., 2009; Arp et al., 2006), that can be attributed to the fact that PFOS has one more -CF_2 moiety than PFOA even though they have the same number of carbon atoms in the carbon chain backbone (ChemAxon, 2020; Ateia et al., 2019).

Electrostatic interaction can also play a role in the adsorptive removal. Due to having very low pKa values (<1), all 4 PFASs remain as anions in the experimental condition of pH ~ 3 (Deng et al., 2012; Goss, 2008; Zhou et al., 2010; Steinle-Darling and Reinhard, 2008; Zhang et al., 2019c). This pH was selected for PFAS removal experiments because it is known as optimum pH for heterogeneous Fenton catalysis (Li et al., 2017; Masud et al., 2020b; Masud et al., 2020a). The plot for zeta potential at different pH values indicates the surface of rGO-nZVI NH and nZVI are positively charged (~22 mV and 21 mV, respectively) at the experimental pH 3, with point of zero charge at ~3.8 (Fig. S3). This suggests that electrostatic interactions between the positively charged rGO-nZVI NH or nZVI and the negatively charged PFASs contribute to the adsorption of PFASs. On the other hand, rGO possessed negative charges (−33 mV) at experimental pH. However, rGO has high adsorptive capacity for PFASs compared to nZVI because of the strong hydrophobic interactions with carbon-based rGO nanosheet, which outweigh the electrostatic repulsion and hence, the Donnan exclusion force. To further elucidate the adsorption mechanism, additional PFOA and PFOS removal tests were carried out at pH 7 (Fig. S4). In the absence of H_2O_2, rGO-nZVI NH performed similar or better adsorptive removal for PFOS and PFOA at pH 7 than at acidic pH 3; although electrostatic repulsion exists between negatively charged rGO-nZVI NH surface (~40 mV) and PFASs at neutral pH. This suggests hydrophobic interactions, instead of electrostatic interactions, could be the dominating adsorptive removal mechanism for rGO-nZVI NH. In addition to hydrophobic interaction, PFAS complexation with oxide/oxyhydroxide surfaces of nZVI can also be attributed to the adsorptive removal of PFASs by rGO-nZVI NH at neutral pH, which cumulatively offset the electrostatic repulsion and results in similar or better PFAS removal compared to acidic pH. (Gao and Chorover, 2012b; Zhang et al., 2018; Wu et al., 2017a; Wu et al., 2017b). In the presence of H_2O_2, however, the PFOA and PFOS removal efficiency of rGO-nZVI NH at pH 7 were respectively 9 % and 11 % lower than that at pH 3 due to the formation of passive oxide layers, and thus, reduced Fenton reactivity at neutral pH (Rezaei and Vione, 2018; Wang et al., 2016; Kecić et al., 2018).

3.2. PFOA and PFOS degradation by rGO-nZVI NH without and with H_2O_2

To identify the PFAS degradation byproducts, individual PFOA and PFOS solutions treated using rGO-nZVI NH with and without H_2O_2 were collected at 0 and 30 min and analyzed using HRMS and IC. Mixed PFASs were not used in this case because the presence of multiple PFASs in the same solution will make it challenging to ascribe the byproducts to their origin and determine the degradation pathways. Because PFOS and PFOA had high removal rate, their degradation byproducts were further identified.

Previous reports discussing PFOA and PFOS have identified shorter chain perfluoroalkyl carboxylic acids (PFCAs) and perfluoroalkyl sulfonic acids (PFSAs) as byproducts of different advanced oxidation/reduction treatment techniques applied to PFOS and PFOA (Park et al., 2016; Gomez-Ruiz et al., 2018; Cui et al., 2020). In ESI- HRMS analysis, PFCAs can be identified by a neutral mass loss, corresponding to CO_2 and characteristic loss of –CF_2 units, with m/z = 118.9925 (which corresponds to CF_3CF_2–) as a common fragment ion observed in the MS^2 spectra. Similarly, PFSAs can be characterized by a loss of the common ions m/z = 79.9573 and 98.9557 during MS^2 fragmentation, corresponding to SO_3– and FSO_3–, respectively (Guardian et al., 2021). However, in the ESI-HRMS analyses of the rGO-nZVI NH-treated PFOS and PFOA samples, all these common fragments of PFCAs and PFSAs were observed only in the same exact retention time of PFOA and PFOS, indicating the absence of any new PFCA and PFSA formed from degradation of PFOA and PFOS.

Instead, two unique masses (m/z 422.9337 and 392.9251) were observed in the HRMS data of the PFOA and PFOS samples treated by rGO-nZVI NH for 30 min – both without and with H_2O_2 (Table 1A). None of these ions were present in the blank samples, or in the initial rGO-nZVI NH-treated PFOA and PFOS samples (collected at 0 min). This indicates the formation of new degradation byproducts during PFOA and PFOS treatment with rGO-nZVI NH. Manual annotation was performed to determine the most probable molecular formula corresponding to each m/z (Table 1A), which appeared to be shorter chain PFAS-Fe complexes: $C_7H_4O_2F_{13}Fe$ (m/z = 422.9337) and $C_6H_2OF_{13}Fe$ (m/z = 392.9251). Metal complexes with organic compounds can be identified in ESI-HRMS based on the isotopic signature of the metal species (Tsednee et al., 2016). Iron is characterized by an isotopic pattern of m/z = 53.93961 (M-2 at 6.3 %), m/z = 55.93494 (M at 100 %), and m/z = 56.9354 (M + 2 at 2.4 %) (Poitrasson, 2011). The isotopic pattern corresponding to an iron-ligand complex was observed in the MS of both of the proposed degradation by products, $C_7H_4O_2F_{13}Fe$ and $C_6H_2OF_{13}Fe$ (Fig. 2), confirming the presence of iron in the complex. Moreover, negative mass defects identified in HRMS (Fig. 2) – often used as a preliminary filter to identify PFAS compounds in non-targeted screening – confirms the presence of fluorinated alkyl moiety in these complexes

Table 1
(A) Summary of the identified degradation byproducts of PFOA and PFOS treated with rGO-nZVI NH and their corresponding identity and peak areas obtained from LC-HRMS analyses. (B) Quantity of formate and acetate detected by IC in PFOA and PFOS samples treated with rGO-nZVI NH. (NF: not found; NH: rGO-nZVI NH).

A. LC-HRMS Results

m/z observed	Proposed Formula [M-H]⁻	mass error, ppm	Peak Area								
			Blank	PFOA				PFOS			
				PFOA only	PFOA + NH + H_2O_2 (0 min)	PFOA + NH (30 min)	PFOA + NH + H_2O_2 (30 min)	PFOS only	PFOS + NH + H_2O_2 (0 min)	PFOS + NH (30 min)	PFOS + NH + H_2O_2 (30 min)
422.9337	$C_7H_4O_2F_{13}Fe$	−4.9	NF	NF	NF	1.68E+07	4.66E+07	NF	NF	7.45E+07	2.21E+08
392.9251	$C_6H_2OF_{13}Fe$	−0.25	NF	NF	NF	1.30E+07	6.36E+07	NF	NF	5.53E+06	2.87E+07

B. Ion Chromatography (IC) Results

Ion	Concentration (ppb) at 30 minutes					
	PFOA Control	PFOA + NH	PFOA + NH + H_2O_2	PFOS Control	PFOS + NH	PFOS + NH + H_2O_2
Formate	NF	Detected (Below LOQ of 5 ppb)	276.3	NF	28.63	433.15
Acetate	NF	Detected (Below LOQ of 2 ppb)	11.73	NF	Detected (Below LOQ of 2 ppb)	25.24

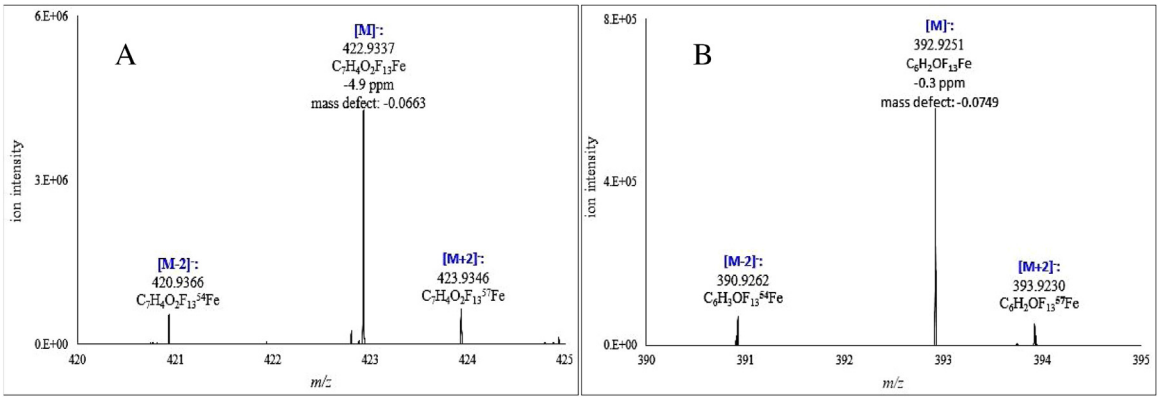

Fig. 2. Experimental isotopic abundance of the precursor ion for the unique *m/z* identified (A: *m/z* = 422.9337; B: *m/z* = 392.9251) during high-resolution mass spectrometry analysis of PFOA and PFOS treated with rGO-nZVI NH. The isotopic pattern confirms presence of Fe in the compound and the negative mass defect confirms presence of fluorinated alkyl moiety.

(Liu et al., 2019; McCord and Strynar, 2019). The MS^2 spectra of these PFAS-Fe complexes and the putative formula of their fragments are shown in Fig. S5. The PFAS-Fe complexes identified here have shorter fluorinated alkyl chains than PFOA and PFOS, confirming degradation by rGO-nZVI NH. The relative abundances of PFAS-complexes were higher in samples treated in the presence of H_2O_2 than in the absence of H_2O_2, which corroborated with the proposed enhancement of degradation by rGO-nZVI- H_2O_2 catalyzed processes.

Previous studies involving nZVI-based removal of PFASs also indicated the possibility of PFAS-Fe complex formation, wherein the degree of complexation was measured by comparing PFAS mass in aqueous phases in the presence and absence of Fe (Park et al., 2018) or by consumption of Fe as monitored by UV–vis spectrometry (Xia and Liu, 2020). In this work, Equations 1–5 present the proposed pathways of PFAS-Fe complex formation of the degradation byproducts identified. The rGO-nZVI NH initiated reduction and oxidation can transform PFOS into PFOA, and in the process, shorten perfluorinated carbon chain releasing two fluorine atoms (Eqs. 1–4) (Singh et al., 2019; Gu et al., 2016). The pathway of desulfurization and hydroxylation of PFOS (Eqs. 1 and 2) followed by defluorination and carboxylation (Eqs. 3 and 4) to form the PFAS-Fe complexes are shown below:

$$(\text{PFOS})\ C_8F_{17}SO_3^- + e^- \rightarrow {}^{\bullet}C_8F_{17} + SO_3^{2-} \quad (1)$$

$$C_8F_{17} + \text{ROS} \rightarrow C_8F_{17}OH \quad (2)$$

$${}^{\bullet}C_8F_{17}OH \rightarrow C_7F_{15}COF + H^+ + F^- \quad (3)$$

$$C_7F_{15}COF + H_2O/\text{ROS} \rightarrow C_7F_{15}COOH + H^+ + F^- \quad (4)$$

The formation pathway of the proposed PFAS-Fe complex resulting from PFOA can be explained in two steps. In the first step, two sequential H/F exchanges occur on α-position C−F bonds (nearest to the functional group) by the reactive species generated by rGO-nZVI NH forming partially defluorinated $C_6F_{13}-CH_2-COOH$

$$(\text{PFOA})\ C_7F_{15}COOH + \text{reactive species} + 2H^+ \rightarrow C_6F_{13}CH_2COOH + 2F^- \quad (5)$$

In the second step, decarboxylation of these partially defluorinated PFASs occur, where the carboxyl functional group is replaced with iron species to form the PFAS-Fe complexes. The two PFAS-Fe complexes that were identified include $[C_6F_{13}Fe(H_2O)]^-$ corresponding to *m/z* = 392.9251, in which both decarboxylation and chain-shortening by one $-CH_2$ moiety occurred, and $[C_6F_{13}CH_2OFe(H_2O)]^-$ corresponding to *m/z* = 422.9337 where only decarboxylation occurred.

The cleavage of the carboxyl functional group can be initiated by ROS generated by rGO-nZVI NH in the presence of H_2O_2, including high valent oxoiron or ferryl species (Shen et al., 1992; Zepp et al., 1992), which ultimately forms these unique PFAS-Fe complexes. As noted previously, these PFAS-Fe complexes were also detected, although in comparatively lower abundance, for removal tests with rGO-nZVI NH in the absence of H_2O_2. This can be attributed to the limited ROS generation capacity of rGO-nZVI NH during corrosion reaction of nZVI with dissolved oxygen of water, even without the presence of H_2O_2 (Wang et al., 2018; Pang et al., 2011). In order to further confirm this mechanism, we characterized the rGO-nZVI NH before and after the PFOA and PFOS removal tests using X-ray diffraction (XRD) and Fourier transform infrared (FTIR) spectroscopy. While the XRD spectrum for rGO-nZVI NH before PFAS removal test (Fig. S6a) shows only a sharp peak for Fe°, the XRD spectra for rGO-nZVI NH after PFAS removal tests show peaks for Fe_2O_3 and β-FeOOH (lepidocrocite) (Vernekar and Jagadeesan, 2015; Wang et al., 2015) in the absence of H_2O_2 and peaks for an amorphous FeOOH (δ-FeOOH) layer (Mei et al., 2015) in the presence of H_2O_2. FTIR spectra (Fig. S6b) show multiple small peaks at ~450−800 cm^{-1} and 1020 cm^{-1} confirming the presence of Fe-O on the rGO-nZVI NH for the treatment solution where H_2O_2 was not present. On the contrary, a much sharper and high intensity peak at 560 cm^{-1} corresponding to Fe-O confirms the higher production of Fe(II)/Fe(III) species on the nZVI surface in the presence of H_2O_2 than in the absence of H_2O_2 (Mei et al., 2015; Tavares et al., 2020).

The proposed pathway for carbon-chain shortening of PFOS and PFOA through decarboxylation can form other byproducts including formate and acetate. Table 1B shows that the quantities of formate and acetate generated by PFAS treatment with rGO-nZVI NH in the presence of H_2O_2 were respectively 1 and 2 orders of magnitude higher than that in the absence of H_2O_2. This observation is consistent with the higher PFAS removal and higher relative abundances of the PFAS-Fe complexes using rGO-nZVI NH with H_2O_2 than in the absence of H_2O_2. Previous studies on PFAS degradation also correlated formate and acetate generation as an indirect measure of PFAS degradation and carbon chain shortening (Singh et al., 2019; Bacha et al., 2019); therefore, the results of formate and acetate generation presented here confirm the proposed mechanism of rGO-nZVI-catalyzed oxidation of PFASs and their enhanced degradation.

In summary, this study presents the potential of rGO-nZVI NH for the enhanced removal and degradation of PFASs. The rGO-nZVI NH exhibited higher efficiencies for PFAS removal than the parent nanomaterials – rGO and nZVI. Long-chain PFOS and PFOA were removed to a greater degree and at a faster rate than short-chain PFPeS and PFPeA. The PFOS and PFOA removal by the rGO-nZVI NH obtained in this study were also faster than similar contemporary micro- and nano-adsorbents that have been listed and compared in Table S3. Most importantly, the treatment of PFOA and PFOS by rGO-nZVI NH yielded unique shorter chain PFAS-Fe complexes – more so in the presence of H_2O_2. The stability and potential for degradation of these unique PFAS-Fe complexes, that have been identified and confirmed for the first time in this study using LC-HRMS analysis, need to be studied further to realize the effectiveness of rGO-NZVI NH based redox treatment in degrading and mineralizing PFASs.

Declaration of competing interest

The authors declare no conflict of interest.

Acknowledgements

This work was partly supported by the Great Lakes Research Consortium (GLRC) Small Grants Award (Award number 77362, Project number 1153633) from the New York State Department of Environmental Conservation to NA.

This work was also supported by the National Science Foundation (Award #1905274 to DSA).

Appendix A. Supplementary data

Supplementary material related to this article can be found, in the online version, at doi:https://doi.org/10.1016/j.hazl.2020.100007.

References

Adusei-Gyamfi, J., Acha, V., 2016. Carriers for nano zerovalent iron (nZVI): synthesis, application and efficiency. RSC Adv. 6 (93), 91025–91044.
Aich, N., Su, C., Kim, I., Masoud, A., 2018. Application of nanozerovalent iron for water treatment and soil remediation: emerging nanohybrid approach and environmental implications. Iron Nanomater. Water Soil Treat. 65–87.
Amirfakhri, S.J., Binny, D., Meunier, J.-L., Berk, D., 2014. Investigation of hydrogen peroxide reduction reaction on graphene and nitrogen doped graphene nanoflakes in neutral solution. J. Power Sources 257, 356–363.
Arp, H.P.H., Niederer, C., Goss, K.-U., 2006. Predicting the partitioning behavior of various highly fluorinated compounds. Environ. Sci. Technol. 40 (23), 7298–7304.
Ateia, M., Maroli, A., Tharayil, N., Karanfil, T., 2019. The overlooked short-and ultrashort-chain poly-and perfluorinated substances: a review. Chemosphere 220, 866–882.
Bacha, A.-U.-R., Nabi, I., Fu, Z., Li, K., Cheng, H., Zhang, L., 2019. A comparative study of bismuth-based photocatalysts with titanium dioxide for perfluorooctanoic acid degradation. Chin. Chem. Lett. 30 (12), 2225–2230.
Bentel, M.J., Yu, Y., Xu, L., Li, Z., Wong, B.M., Men, Y., Liu, J., 2019. Defluorination of per- and polyfluoroalkyl substances (PFASs) with hydrated electrons: structural dependence and implications to PFAS remediation and management. Environ. Sci. Technol. 53 (7), 3718–3728.
ChemAxon. https://chemicalize.com (Accessed October 05, 2020).
Chen, Y.-C., Lo, S.-L., Kuo, J., 2011. Effects of titanate nanotubes synthesized by a microwave hydrothermal method on photocatalytic decomposition of perfluorooctanoic acid. Water Res. 45 (14), 4131–4140.
Cui, J., Gao, P., Deng, Y., 2020. Destruction of per- and polyfluoroalkyl substances (PFAS) with advanced reduction processes (ARPs): a critical review. Environ. Sci. Technol. 54 (7), 3752–3766.
Deng, S., Zhang, Q., Nie, Y., Wei, H., Wang, B., Huang, J., Yu, G., Xing, B., 2012. Sorption mechanisms of perfluorinated compounds on carbon nanotubes. Environ. Pollut. 168, 138–144.
DeWitt, J.C., 2015. Toxicological Effects of Perfluoroalkyl and Polyfluoroalkyl Substances. Springer.
Düzenli, D., 2016. A comparative density functional study of hydrogen peroxide adsorption and activation on the graphene surface doped with N, B, S, Pd, Pt, Au, Ag, and Cu atoms. J. Phys. Chem. C 120 (36), 20149–20157.
Gallen, C., Eaglesham, G., Drage, D., Nguyen, T.H., Mueller, J., 2018. A mass estimate of perfluoroalkyl substance (PFAS) release from Australian wastewater treatment plants. Chemosphere 208, 975–983.
Gao, X., Chorover, J., 2012a. Adsorption of perfluorooctanoic acid and perfluorooctanesulfonic acid to iron oxide surfaces as studied by flow-through ATR-FTIR spectroscopy. Environ. Chem. 9 (2), 148–157.
Gao, X.D., Chorover, J., 2012b. Adsorption of perfluorooctanoic acid and perfluorooctanesulfonic acid to iron oxide surfaces as studied by flow-through ATR-FTIR spectroscopy. Environ. Chem. 9 (2), 148–157.
Gomez-Ruiz, B., Ribao, P., Diban, N., Rivero, M.J., Ortiz, I., Urtiaga, A., 2018. Photocatalytic degradation and mineralization of perfluorooctanoic acid (PFOA) using a composite TiO2 −rGO catalyst. J. Hazard. Mater. 344, 950–957.
Goss, K.-U., 2008. The pKa values of PFOA and other highly fluorinated carboxylic acids. Environ. Sci. Technol. 42 (2), 456–458.
Gu, Y., Dong, W., Luo, C., Liu, T., 2016. Efficient reductive decomposition of perfluorooctanesulfonate in a high photon flux UV/sulfite system. Environ. Sci. Technol. 50 (19), 10554–10561.
Gu, M., Farooq, U., Lu, S., Zhang, X., Qiu, Z., Sui, Q., 2018. Degradation of trichloroethylene in aqueous solution by rGO supported nZVI catalyst under several oxic environments. J. Hazard. Mater. 349, 35–44.
Guardian, M.G.E., Boongaling, E.G., Bernardo-Boongaling, V.R.R., Gamonchuang, J., Boontongto, T., Burakham, R., Arnnok, P., Aga, D.S., 2020. Prevalence of per-and polyfluoroalkyl substances (PFASs) in drinking and source water from two Asian countries. Chemosphere 127115.
Guardian, M.G.E., Antle, J.P., Vexelman, P.A., Aga, D.S., Simpson, S.M., 2021. Resolving unknown isomers of emerging per- and polyfluoroalkyl substances (PFASs) in environmental samples using COSMO-RS-derived retention factor and mass fragmentation patterns. J. Hazard. Mater. 402123478.
Gui, D., Zhang, M., Zhang, T., Zhang, B., Lin, W., Sun, X., Yu, X., Liu, W., Wu, Y., 2019. Bioaccumulation behavior and spatiotemporal trends of per-and polyfluoroalkyl substances in Indo-Pacific humpback dolphins from the Pearl River Estuary, China. Sci. Total Environ. 658, 1029–1038.
Hekster, F.M., Laane, R.W., de Voogt, P., 2003. Environmental and toxicity effects of perfluoroalkylated substances. Reviews of Environmental Contamination and Toxicology. Springer, pp. 99–121.
Jang, B., Chae, O.B., Park, S.-K., Ha, J., Oh, S.M., Na, H.B., Piao, Y., 2013. Solventless synthesis of an iron-oxide/graphene nanocomposite and its application as an anode in high-rate Li-ion batteries. J. Mater. Chem. A 1 (48), 15442–15446.
Kaboré, H.A., Duy, S.V., Munoz, G., Méité, L., Desrosiers, M., Liu, J., Sory, T.K., Sauvé, S., 2018. Worldwide drinking water occurrence and levels of newly-identified perfluoroalkyl and polyfluoroalkyl substances. Sci. Total Environ. 616, 1089–1100.
Kecić, V., Kerkez, Đ., Prica, M., Lužanin, O., Bečelić-Tomin, M., Pilipović, D.T., Dalmacija, B., 2018. Optimization of azo printing dye removal with oak leaves-nZVI/H2O2 system using statistically designed experiment. J. Clean. Prod. 202, 65–80.

Kelly, B.C., Ikonomou, M.G., Blair, J.D., Surridge, B., Hoover, D., Grace, R., Gobas, F.A., 2009. Perfluoroalkyl contaminants in an Arctic marine food web: trophic magnification and wildlife exposure. Environ. Sci. Technol. 43 (11), 4037–4043.
Kim, M., Li, L.Y., Grace, J.R., Yue, C., 2015. Selecting reliable physicochemical properties of perfluoroalkyl and polyfluoroalkyl substances (PFASs) based on molecular descriptors. Environ. Pollut. 196, 462–472.
Kucharzyk, K.H., Darlington, R., Benotti, M., Deeb, R., Hawley, E., 2017. Novel treatment technologies for PFAS compounds: a critical review. J. Environ. Manage. 204, 757–764.
Lau, C., Thibodeaux, J.R., Hanson, R.G., Narotsky, M.G., Rogers, J.M., Lindstrom, A.B., Strynar, M.J., 2006. Effects of perfluorooctanoic acid exposure during pregnancy in the mouse. Toxicol. Sci. 90 (2), 510–518.
Li, S., Zhang, G., Zhang, W., Zheng, H., Zhu, W., Sun, N., Zheng, Y., Wang, P., 2017. Microwave enhanced Fenton-like process for degradation of perfluorooctanoic acid (PFOA) using Pb-BiFeO3/rGO as heterogeneous catalyst. Chem. Eng. J. 326, 756–764.
Liu, Y., D'Agostino, L.A., Qu, G., Jiang, G., Martin, J.W., 2019. High-resolution mass spectrometry (HRMS) methods for nontarget discovery and characterization of poly- and per-fluoroalkyl substances (PFASs) in environmental and human samples. TrAC Trends Anal. Chem. 121115420.
Majidi, R., Karami, A., 2014. Hydrogen peroxide adsorption on graphene with stone-wales defect. J. Nanostruct. 4 (1), 1–8.
Masud, A., Cui, Y., Atkinson, J.D., Aich, N., 2018. Shape matters: Cr (VI) removal using iron nanoparticle impregnated 1-D vs 2-D carbon nanohybrids prepared by ultrasonic spray pyrolysis. J. Nanopart. Res. 20 (3), 64.
Masud, A., Soria, N.G.C., Aga, D.S., Aich, N., 2020a. Adsorption and advanced oxidation of diverse pharmaceuticals and personal care products (PPCPs) from water using highly efficient rGO-nZVI Nanohybrids. Environ. Sci. Water Res. Technol. .
Masud, A., Soria, N.G.C., Aga, D.S., Aich, N., 2020b. Adsorption and advanced oxidation of diverse pharmaceuticals and personal care products (PPCPs) from water using highly efficient rGO–nZVI nanohybrids. Environ. Sci. Water Res. Technol. 6 (8), 2223–2238.
McCord, J., Strynar, M., 2019. Identifying per-and polyfluorinated chemical species with a combined targeted and non-targeted-screening high-resolution mass spectrometry workflow. JoVE 146e59142.
Mehrabi, N., Masud, A., Afolabi, M., Hwang, J., Calderon Ortiz, G.A., Aich, N., 2019. Magnetic graphene oxide-nano zero valent iron (GO–nZVI) nanohybrids synthesized using biocompatible cross-linkers for methylene blue removal. RSC Adv. 9 (2), 963–973.
Mei, L.F., Liao, L.B., Wang, Z.S., Xu, C.C., 2015. Interactions between phosphoric/tannic acid and different forms of FeOOH. Adv. Mater. Sci. Eng. 2015.
Meng, P., Deng, S., Lu, X., Du, Z., Wang, B., Huang, J., Wang, Y., Yu, G., Xing, B., 2014. Role of air bubbles overlooked in the adsorption of perfluorooctanesulfonate on hydrophobic carbonaceous adsorbents. Environ. Sci. Technol. 48 (23), 13785–13792.
Pang, S.-Y., Jiang, J., Ma, J., 2011. Oxidation of sulfoxides and arsenic(III) in corrosion of nanoscale zero valent iron by oxygen: evidence against Ferryl Ions (Fe(IV)) as active intermediates in Fenton reaction. Environ. Sci. Technol. 45 (1), 307–312.
Parenky, A.C., Gevaerd de Souza, N., Asgari, P., Jeon, J., Nadagouda, M.N., Choi, H., 2020. Removal of perfluorooctanesulfonic acid in water by combining zerovalent iron particles with common oxidants. Environ. Eng. Sci. .
Park, S., Lee, L.S., Medina, V.F., Zull, A., Waisner, S., 2016. Heat-activated persulfate oxidation of PFOA, 6:2 fluorotelomer sulfonate, and PFOS under conditions suitable for in-situ groundwater remediation. Chemosphere 145, 376–383.
Park, S., Zenobio, J.E., Lee, L.S., 2018. Perfluorooctane sulfonate (PFOS) removal with Pd0/nFe0 nanoparticles: Adsorption or aqueous Fe-complexation, not transformation? J. Hazard. Mater. 342, 20–28.
Peik-See, T., Pandikumar, A., Ngee, L.H., Ming, H.N., Hua, C.C., 2014. Magnetically separable reduced graphene oxide/iron oxide nanocomposite materials for environmental remediation. Catal. Sci. Technol. 4 (12), 4396–4405.
Poitrasson, F., 2011. Iron isotopes. In: Gargaud, M., Amils, R., Quintanilla, J.C., Cleaves, H. J., Irvine, W.M., Pinti, D.L., Viso, M. (Eds.), Encyclopedia of Astrobiology. Springer Berlin Heidelberg, Berlin, Heidelberg, pp. 852–855.
Post, G.B., Louis, J.B., Lippincott, R.L., Procopio, N.A., 2013. Occurrence of perfluorinated compounds in raw water from New Jersey public drinking water systems. Environ. Sci. Technol. 47 (23), 13266–13275.
Rezaei, F., Vione, D., 2018. Effect of pH on zero valent Iron performance in heterogeneous Fenton and Fenton-like processes: a review. Molecules 23 (12) .
Saleh, N.B., Khalid, A., Tian, Y., Ayres, C., Sabaraya, I.V., Pietari, J., Hanigan, D., Chowdhury, I., Apul, O.G., 2019. Removal of poly-and per-fluoroalkyl substances from aqueous systems by nano-enabled water treatment strategies. Environ. Sci. Water Res. Technol. 5 (2), 198–208.
Shen, X., Tian, J., Li, J., Li, X., Chen, Y., 1992. Formation of the excited ferryl species following Fenton reaction. Free Radic. Biol. Med. 13 (5), 585–592.
Singh, R.K., Fernando, S., Baygi, S.F., Multari, N., Thagard, S.M., Holsen, T.M., 2019. Breakdown products from perfluorinated alkyl substances (PFAS) degradation in a plasma-based water treatment process. Environ. Sci. Technol. 53 (5), 2731–2738.
Steinle-Darling, E., Reinhard, M., 2008. Nanofiltration for trace organic contaminant removal: structure, solution, and membrane fouling effects on the rejection of perfluorochemicals. Environ. Sci. Technol. 42 (14), 5292–5297.
Tavares, T.S., da Rocha, E.P., Nogueira, F.G.E., Torres, J.A., Silva, M.C., Kuca, K., Ramalho, T.C., 2020. Delta-FeOOH as support for immobilization peroxidase: optimization via a chemometric approach. Molecules 25 (2) .
Tsednee, M., Huang, Y.-C., Chen, Y.-R., Yeh, K.-C., 2016. Identification of metal species by ESI-MS/MS through release of free metals from the corresponding metal-ligand complexes. Sci. Rep. 6 (1), 1–13.
Vernekar, D., Jagadeesan, D., 2015. Tunable acid-base bifunctional catalytic activity of FeOOH in an orthogonal tandem reaction. Catal. Sci. Technol. 5 (8), 4029–4038.
Wang, X.M., Zhu, M.Q., Lan, S., Ginder-Vogel, M., Liu, F., Feng, X.H., 2015. Formation and secondary mineralization of ferrihydrite in the presence of silicate and Mn(II). Chem. Geol. 415, 37–46.
Wang, L., Yang, J., Li, Y., Lv, J., Zou, J., 2016. Removal of chlorpheniramine in a nanoscale zero-valent iron induced heterogeneous Fenton system: Influencing factors and degradation intermediates. Chem. Eng. J. 284, 1058–1067.
Wang, Q., Masud, A., Aich, N., Wu, Y., 2018. In Vitro pulmonary toxicity of reduced graphene oxide-nano zero valent iron nanohybrids and comparison with parent nanomaterial attributes. ACS Sustain. Chem. Eng. 6 (10), 12797–12806.
Wu, C., Tu, J., Liu, W., Zhang, J., Chu, S., Lu, G., Lin, Z., Dang, Z., 2017a. The double influence mechanism of pH on arsenic removal by nano zero valent iron: electrostatic interactions and the corrosion of Fe0. Environ. Sci. Nano 4 (7), 1544–1552.
Wu, C., Tu, J.W., Liu, W.Z., Zhang, J., Chu, S.Q., Lu, G.N., Lin, Z., Dang, Z., 2017b. The double influence mechanism of pH on arsenic removal by nano zero valent iron: electrostatic interactions and the corrosion of Fe-0. Environ. Sci. -Nano 4 (7), 1544–1552.
Xia, C., Liu, J., 2020. Degradation of perfluorooctanoic acid by zero-valent iron nanoparticles under ultraviolet light. J. Nanopart. Res. 22 (7), 1–13.
Xu, L., Wang, J., 2011. A heterogeneous Fenton-like system with nanoparticulate zero-valent iron for removal of 4-chloro-3-methyl phenol. J. Hazard. Mater. 186 (1), 256–264.
Xue, A., Yuan, Z.-W., Sun, Y., Cao, A.-Y., Zhao, H.-Z., 2015. Electro-oxidation of perfluorooctanoic acid by carbon nanotube sponge anode and the mechanism. Chemosphere 141, 120–126.
Zepp, R.G., Faust, B.C., Hoigne, J., 1992. Hydroxyl radical formation in aqueous reactions (pH 3-8) of iron(II) with hydrogen peroxide: the photo-Fenton reaction. Environ. Sci. Technol. 26 (2), 313–319.
Zhang, Y., Zhi, Y., Liu, J., Ghoshal, S., 2018. Sorption of perfluoroalkyl acids to fresh and aged nanoscale zerovalent iron particles. Environ. Sci. Technol. 52 (11), 6300–6308.
Zhang, W., Zhang, D., Liang, Y., 2019a. Nanotechnology in remediation of water contaminated by poly-and perfluoroalkyl substances: a review. Environ. Pollut. 247, 266–276.
Zhang, D., He, Q., Wang, M., Zhang, W., Liang, Y., 2019b. Sorption of perfluoroalkylated substances (PFASs) onto granular activated carbon and biochar. Environ. Technol. 1–12.
Zhang, D.Q., Zhang, W.L., Liang, Y.N., 2019c. Adsorption of perfluoroalkyl and polyfluoroalkyl substances (PFASs) from aqueous solution - a review. Sci. Total Environ. 694133606.
Zhao, X., Liu, W., Cai, Z., Han, B., Qian, T., Zhao, D., 2016a. An overview of preparation and applications of stabilized zero-valent iron nanoparticles for soil and groundwater remediation. Water Res. 100, 245–266.
Zhao, C., Fan, J., Chen, D., Xu, Y., Wang, T., 2016b. Microfluidics-generated graphene oxide microspheres and their application to removal of perfluorooctane sulfonate from polluted water. Nano Res. 9 (3), 866–875.
Zhou, Q., Deng, S., Yu, Q., Zhang, Q., Yu, G., Huang, J., He, H., 2010. Sorption of perfluorooctane sulfonate on organo-montmorillonites. Chemosphere 78 (6), 688–694.